AGU PUBLICATIONS

Geophysical Research Letters

RESEARCH LETTER
10.1002/2015GL063988

Isotope meteorology of cold front passages: A case study combining observations and modeling

F. Aemisegger[1,2], J. K. Spiegel[3], S. Pfahl[1], H. Sodemann[1,4], W. Eugster[3], and H. Wernli[1]

[1]Institute for Atmospheric and Climate Science, ETH Zurich, Zurich, Switzerland, [2]Centre for Environmental and Climate Research, Lund University, Lund, Sweden, [3]Institute of Agricultural Sciences, ETH Zurich, Zurich, Switzerland, [4]Geophysical Institute, University of Bergen, Bergen, Norway

Abstract This study investigates the role of below-cloud evaporation and evapotranspiration for the short-term variability of stable isotopes in near-surface water vapor and precipitation associated with central European cold fronts. To this end, a combination of observations with high temporal resolution and numerical sensitivity experiments with the isotope-enabled regional weather prediction model $COSMO_{iso}$ is used. The representation of the interaction between rain droplets and ambient vapor below the cloud is fundamental for adequately simulating precipitation isotopes (δ_p) and total rainfall amount. Neglecting these effects leads to depletion biases of 20–40‰ in δ_p^2H and 5–10‰ in $\delta_p^{18}O$ and to an increase of 74% in rainfall amount. Isotope fractionation during soil evaporation is of primary importance for correctly simulating the variability of continental low-level vapor δ_v^2H and $\delta_v^{18}O$ and particularly of the secondary isotope parameter deuterium excess (d_v).

Key Points:
- Cold fronts leave characteristic imprint in water vapor and rain isotopes
- Below-cloud interaction affects rainfall amount and precipitation isotopes at short time scales
- Soil evaporation fractionation is crucial for isotopes in low-level water vapor

Supporting Information:
- Captions for Figures S1–S6
- Text S1
- Figure S1
- Figure S2
- Figure S3
- Figure S4
- Figure S5
- Figure S6

Correspondence to:
F. Aemisegger,
franziska.aemisegger@usys.ethz.ch

Citation:
Aemisegger, F., J. K. Spiegel, S. Pfahl, H. Sodemann, W. Eugster, and H. Wernli (2015), Isotope meteorology of cold front passages: A case study combining observations and modeling, *Geophys. Res. Lett.*, *42*, 5652–5660, doi:10.1002/2015GL063988.

Received 27 MAR 2015
Accepted 19 JUN 2015
Accepted article online 24 JUN 2015
Published online 14 JUL 2015

1. Introduction

The adequate representation of precipitation in a limited-area numerical model depends on the correct simulation of a large number of processes involving several spatial and temporal scales [*Rossa et al.*, 2008]. In this respect, a proper description of surface evaporation at the remote moisture source (in this study in particular soil evaporation, SE), large-scale water vapor transport [e.g., *Winschall et al.*, 2012; *Grams et al.*, 2014], cloud microphysics, and local below-cloud (BC) interaction between rainfall and ambient water vapor [e.g., *Dawson et al.*, 2010] is crucial. Due to the lack of direct measurements of several of the variables involved in these dynamically relevant processes, the verification of their correct representation in the model is challenging.

Stable isotopes of water in vapor and precipitation record the phase change history of a water sample [*Dansgaard*, 1964]. Isotopes in water vapor (δ_v^2H, $\delta_v^{18}O$, deuterium excess $d_v = \delta_v^2H - 8 \cdot \delta_v^{18}O$) and precipitation ($\delta_p^2H$, $\delta_p^{18}O$, $d_p = \delta_p^2H - 8 \cdot \delta_p^{18}O$) thus provide a measurable constraint on the processes involved in vapor and precipitation formation (see *Coplen* [2011], for details on the isotope notation and standardization). A prerequisite for a meaningful application of this additional observational constraint is a proper understanding of the mechanisms controlling isotopic variations during the passage of specific weather systems like midlatitude fronts.

Frontal passages are typically associated with intense precipitation. Few studies have specifically investigated the characteristic isotope signature of those weather systems in vapor and precipitation [*Gedzelman and Lawrence*, 1990; *Pfahl et al.*, 2012]. Existing studies mainly concentrate on explaining the observed temporal evolution in the δ_p signals and associate these with different cloud types (e.g., convective or stratiform) [*Miyake et al.*, 1968; *Rindsberger et al.*, 1990; *Celle-Jeanton et al.*, 2004; *Coplen et al.*, 2008; *Risi et al.*, 2008; *Barras and Simmonds*, 2009; *Yoshimura et al.*, 2010; *Muller et al.*, 2015]. Processes at three different scales control the spatial and temporal evolution of isotopes in vapor and precipitation during a cold front passage [*Barras and Simmonds*, 2009; *Pfahl et al.*, 2012]: (i) the large-scale properties of air masses corresponding to the climatological isotope effects described by *Dansgaard* [1964]; (ii) the contribution of the weather system, here the cold front; and (iii) the microphysical interaction between vapor and rain droplets below the clouds, bringing the isotopic composition of the rain closer to equilibrium with BC vapor in saturated regions or enriching the rain droplets in regions with relative humidity below 100%. So far, the relevance of each of these groups of processes as well as their interaction has not yet been sufficiently constrained.

In this paper, the importance of these three groups of processes is investigated in a case study of simultaneous water vapor and precipitation isotope measurements (see section 2) during the passage of cold fronts combined with simulations with the isotope-enabled regional numerical weather prediction model $COSMO_{iso}$. We first discuss the role of the cold fronts that passed our measurement site during a 1 week campaign for the variability of the measured isotope signals (section 3.1) and then outline possible reasons for the observed disequilibrium between the vapor and the liquid phase in our measurements (section 3.2). Finally, we examine the relative importance of remote (SE) and local (BC) isotope fractionation effects during the passage of one of the observed cold fronts with $COSMO_{iso}$ experiments (section 4).

2. Isotope Measurements

Isotope measurements in ambient water vapor were performed in Zurich (47.38°N, 8.55°E, 500 m above sea level) between 19 and 25 July 2011 with a cavity ring-down spectrometer Picarro L1115-i. Hourly averages of 5 s measurements are used here with an estimated total uncertainty of 0.8‰ for δ^2H and 0.2‰ for δ^{18}O after calibration (see *Aemisegger et al.* [2012], for more details about the setup, calibration procedure, and the measurement uncertainties). At the same location, precipitation was sampled with an automatic sequential rainfall sampler previously used for studies of wet deposition of solutes in rainfall [*Eugster et al.*, 1998]. Precipitation was collected in 50 mL bottles inserted into a carousel that advanced the bottles every hour to provide 1 h resolution during events with a precipitation rate above 1 mm h^{-1}. The accumulation time was longer if the required minimum hourly precipitation amount was not reached. The lid of the sampler closed automatically after 1 min when no rainfall was detected to minimize potential isotope fractionation due to postsampling evaporation. This is similar to the concept chosen by *Coplen et al.* [2008] who also tried to minimize evaporation with their sampler design. The rainfall samples were gathered on the morning of the 20, 23, and 24 July and analyzed in the laboratory for their isotopic composition with a Picarro L2130-i instrument, an A0212 vaporizer operated in high-precision mode and an autosampler (precision 0.1‰ for δ_p^2H and 0.03‰ for δ_p^{18}O). The estimated overall uncertainty taking into account collection and handling (evaporative effects) is 2‰ for δ_p^2H and 1‰ for δ_p^{18}O. This estimate is based on average values obtained from measurements of bottles filled with 25 mL of a known liquid water standard and left in the rainfall sampler as a control between two collection times (see also the more detailed laboratory study by *Prechsl et al.* [2014]). Note that d_p measurements are thus affected by large uncertainties and possibly also by small biases due to evaporation during sample collection. Other meteorological variables including precipitation intensity, 2 m temperature, and relative humidity were measured at the MeteoSwiss station, Fluntern, nearby.

3. Simultaneous Water Vapor and Precipitation Isotope Measurements

3.1. Frontal Precipitation Systems Strongly Modulate Isotope Signals

Four rainfall episodes occurred in Zurich during the 1 week of measurements between 19 and 25 July. The week was characterized by fairly low summer temperatures (between 9°C and 20°C) and precipitation due the passage of two cold fronts (at about 18 UTC 19 July and 00 UTC 24 July) and due to shallow convection in relatively cool air beneath an upper level trough between 21 and 23 July. In terms of precipitation intensity, the rainfall episodes are comparable, all with peak hourly values of 5–8 mm hr^{-1} and event accumulated values exceeding 10 mm. The passage of the cold front at 00 UTC 24 July and a general protrusion of cold air from the North Atlantic toward the Mediterranean and Eastern Europe are clearly visible in Figure 1, together with a cyclonic low-level circulation in the North Sea and a pronounced anticyclone over northern Africa. Figure S1 in the supporting information visualizes the meteorological evolution for the entire measurement period and confirms the generally cool conditions over Central Europe.

The water isotope measurements clearly reflect the influence of the aforementioned weather systems with relatively higher δ_v values in the period 12UTC 21 July to 12UTC 22 July and lower δ_v values after the cold fronts pass (Figure 2). The passing of the cold fronts on 19 and 24 July are reflected by a characteristic V shape in the δ_v signals (Figure 2). In both cases, a rapid and strong decrease in the isotope observations (≈8–10‰h^{-1} in δ_v^2H and ≈ 1°h^{-1} in δ_v^{18}O) is followed by a slower recovery of the δ_v signals reaching a plateau value, which is lower than the δ_v signature of the warm air mass before the passage of the cold front. The decreases observed in δ_p are of the same magnitude as in δ_v. Additional short-term variability can be observed in the δ_p^{18}O samples during the cold front passages. The minima in δ_v and δ_p occur at the same time or shortly after the precipitation intensity peak on 19 and 24 July. Similar patterns of a V-shaped decrease have also been observed elsewhere in frontal precipitation [*Miyake et al.*, 1968; *Gedzelman and Lawrence*, 1990; *Celle-Jeanton et al.*, 2004;

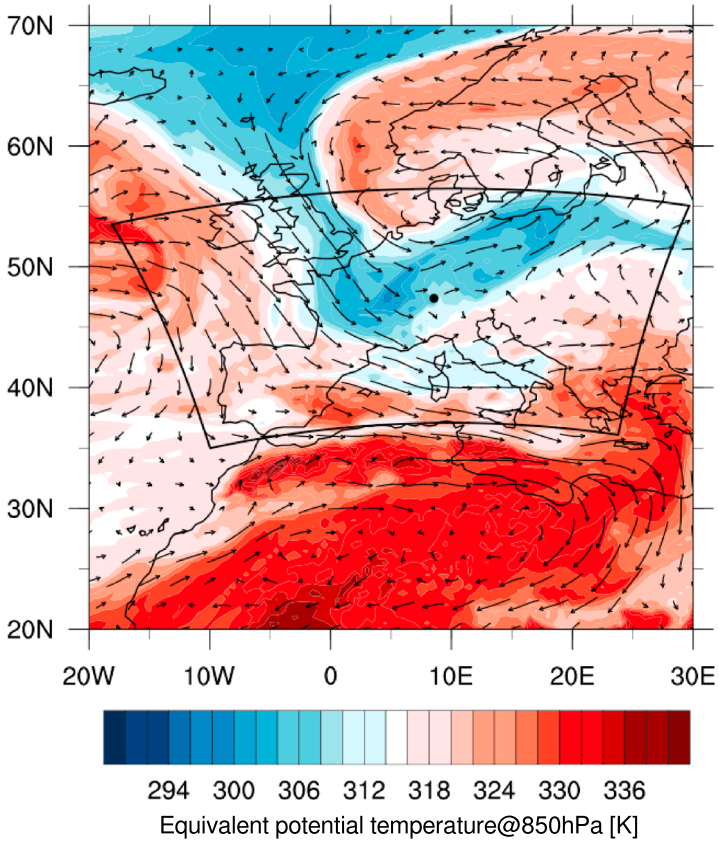

Figure 1. Equivalent potential temperature (contour colors) and horizontal wind (arrows) at 850 hPa from ECMWF analysis data at 00UTC 24 July 2011 for Europe. Zurich is marked with a black dot. The computational domain of the $COSMO_{iso}$ simulations is shown by the black box. The temporal evolution of the weather situation between 18UTC 19 July and 00UTC 24 July 2011 is shown in Figure S1 in the supporting information.

Coplen et al., 2008; *Risi et al.*, 2008; *Barras and Simmonds*, 2009] and in cloud water [*Spiegel et al.*, 2012]. The temporal evolution of d_v and d_p during the two cold front passages is not as characteristic as that of δ_v and δ_p. The minima in δ_v coincide with a short-term maximum in d_v.

In contrast, the convective precipitation period induced by the upper level trough between 12UTC 21 July and 12UTC 22 July (see Figure S2) is characterized by gradually more enriched δ_v values, reflecting the influence of the warmer air mass from the south. This increase is also present in δ_p.

It is important to note that in our measurements no clear diel cycle is visible (except for d_v on 24–25 July, see section 4.2). The complex large-scale flow situation determines the temporal evolution of the isotope signals observed during this campaign rather than the daily cycle of local surface fluxes and boundary layer mixing, which were discernible in previous studies [e.g. *Lee et al.*, 2005].

3.2. Disequilibrium Between Vapor and Precipitation Isotopes

Over the whole campaign, we find relatively strong linear correlations between the vapor isotope and precipitation isotope measurements ($r_{vp}(\delta^{18}O) = 0.56$ and $r_{vp}(\delta^{2}H) = 0.80$ at p values < 0.01, see scatter plots in Figure S3). High r_{vp} values can result from two different causes. First, high correlations can arise from the fact that near-surface δ_v signals are linked with the evolution of δ_v at higher altitudes where precipitation is formed. In this case, the isotope signatures of the two phases evolve similarly in time due to the linkage with the large-scale flow. Near-surface vapor and higher-altitude vapor thus would have the same moisture source and a similar transport history. Second, the fact that δ_p and δ_v covary in time can be due to BC interaction inducing isotopic equilibration between BC vapor and precipitation. Several strongly negative d_p values in combination with a much lower variability in d_v point toward an important contribution from evaporative BC effects (evaporative BC effects decrease d_p, whereas they tend to increase d_v). In fact, d_v and d_p are not as well correlated as the δ signals ($r_{vp}(d) = 0.36$, at p value = 0.05), which is in line with this interpretation. However,

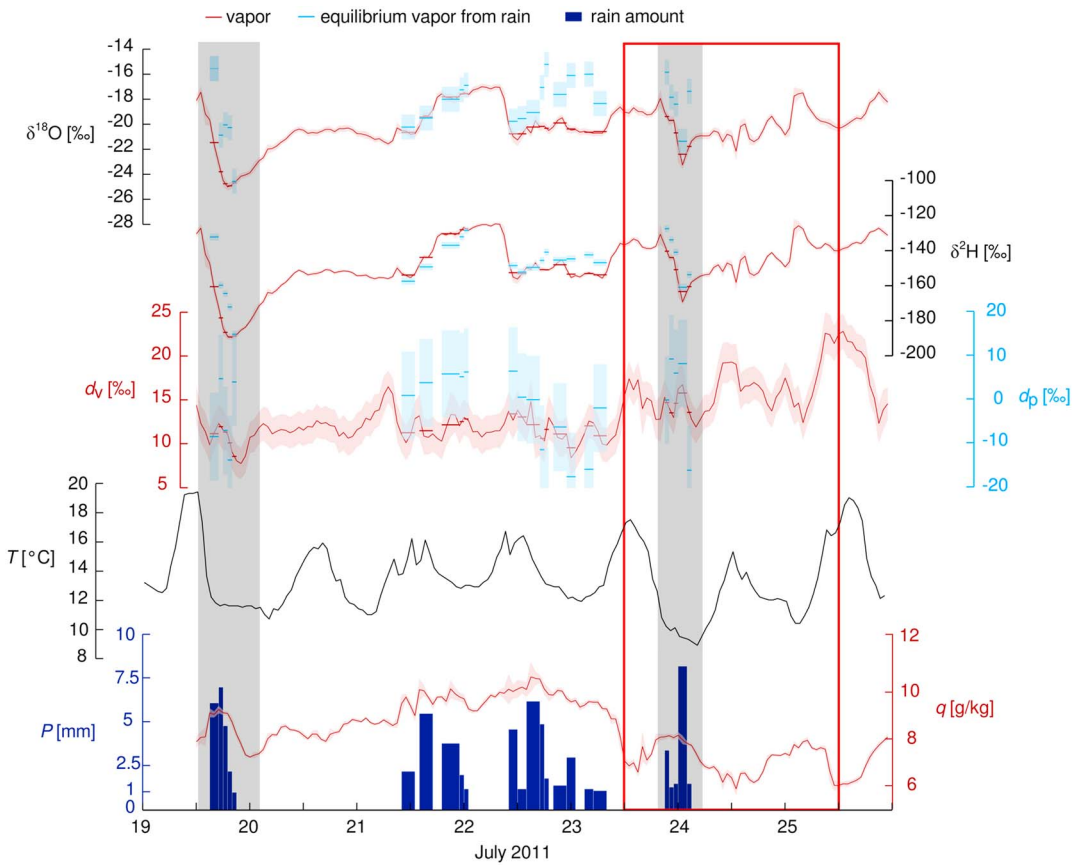

Figure 2. Overview of the hourly measurements of δ_v^2H, δ_v^{18}O, and d_v in near-surface water vapor (red) and equilibrium vapor from sampled rain water ($\delta_{veqp}{}^2$H, $\delta_{veqp}{}^{18}$O, and d_{veqp}, light blue) between 19 July 2011 and 25 July 2011 in Zurich, Switzerland. The shaded red area indicates the uncertainty range of the water vapor isotope measurements. The equilibrium vapor data from the collected rainfall sample were calculated using the measured 2 m temperature and the equilibrium fractionation factors from *Majoube* [1971]. The rainfall sampling intervals are indicated by the length of the short blue lines. The short red lines show the average isotopic composition of vapor weighted by the water vapor mixing ratio for the corresponding rainfall sampling intervals. In the two bottom panels the 2 m temperature, the measured hourly specific humidity q, and the precipitation amount for the rainfall sampling intervals are shown. Date ticks are at 00 and 12UTC. The grey shaded areas indicate cold front passages. The red frame indicates the period simulated with $COSMO_{iso}$.

the lower $r_{vp}(d)$ value might also be compromised by the much higher uncertainties in d than in the δ signals. Even though the measured relative humidity at the ground was high (> 84%) during the rainfall periods, the weak rainfall intensities (small droplets and thus lower falling velocities [*Lee and Fung*, 2007]), and the possibly lower relative humidity in the air column above could have contributed to the evaporative enrichment of precipitation. The importance of BC effects for the cold front passage at 00UTC 24 July is quantified and further discussed in section 4 below.

The departure from isotopic equilibrium between the vapor and the liquid phase ($\delta_v - \delta_{veqp}$) can be a helpful measure for understanding the cause of the strong link between δ_p and δ_v. The rainfall and low-level water vapor samples measured here are generally not in isotopic equilibrium (compare red and blue lines in Figure 2). On average the vapor samples are 4.5‰ more depleted in δ^2H and 2‰ more depleted in δ^{18}O compared to the equilibrium vapor from precipitation (δ_{veqp}). In addition to the relative enrichment of precipitation due to BC rain evaporation, a dynamical effect causing an inverse vertical gradient in δ_v could explain the presence of more depleted vapor at the ground than at the level of cloud formation aloft. The vertical structure of a typical cold front, inducing warm air to rise along the backward sloping front, implies that the water vapor forming precipitation could be predominantly originating from the warm sector. Near the surface, the cold front has already progressed beyond the measurement location, and more depleted water vapor from the cold sector is measured. Orographic lifting or upper level troughs could lead to a similar

variability in the vertical water vapor isotope profile (an example of the complex vertical structures of δ_v from a $COSMO_{iso}$ simulation is shown in Figure S4).

Previous studies, for which no measurements in water vapor were available, deduced δ_v by assuming isotopic equilibrium with measured precipitation values [*Bowen and Revenaugh*, 2003; *Gibson et al.*, 2008; *Jasechko et al.*, 2013]. During our campaign, the difference between the average δ_v weighted by the water vapor mixing ratio (during rainy and dry periods) and δ_{veqp} weighted by the rain rate is −1.4‰ for $\delta^{18}O$, 1.4‰ for δ^2H and 12.8‰ for d. The errors made with an equilibrium assumption would thus be negligible compared to the measurement uncertainty for δ but not for d (see section 2). Longer-term simultaneous precipitation and water vapor measurements with high temporal resolution at different stations are needed to robustly quantify the disequilibrium between the two phases as well as its possible seasonality and variability in space.

4. Comparison Between Isotope Measurements and $COSMO_{iso}$ Simulations

4.1. Description of the $COSMO_{iso}$ Simulations and Sensitivity Experiments

To quantitatively investigate the role of different isotopic fractionation processes, sensitivity studies have been carried out with $COSMO_{iso}$ at a horizontal resolution of 7 km (see *Steppeler et al.* [2003] for details about the limited-area model in general and *Pfahl et al.* [2012] for details about the water isotope implementation). $COSMO_{iso}$ is run with the TERRA-ML soil-vegetation-atmosphere transfer scheme [*Schrodin and Heise*, 2001; *Grasselt et al.*, 2008], which is also used in operational weather forecasting with COSMO. The following settings for (i) below-cloud evaporation (BC) and (ii) soil evaporation (SE) were used in these model experiments:

1. BC0: Isotope fractionation and equilibration during BC interaction is switched off in these simulations (similar to *Pfahl et al.* [2012]). The isotope ratio of the evaporation flux from rain droplets is assumed to be equal to the composition of the rain. The isotope ratio of the rain droplets is thus kept constant below the cloud.
2. BC1: Simulation including BC interaction (see *Pfahl et al.* [2012], for details on parameterizations).
3. SE0: Simulation without fractionation during evapotranspiration, similar to most isotope-enabled atmospheric general circulation models (GCM) [*Hoffmann et al.*, 1998; *Yoshimura et al.*, 2008]. The evapotranspiration flux has the same isotope ratio as the soil moisture taken from the global model (see below).
4. SE1: Simulation with fractionation during SE following *Craig and Gordon* [1965]; transpiration is assumed to be nonfractionating; the soil water isotopes are taken from the global model.

Simulations have been performed for all combinations of BC and SE settings. The initial and boundary conditions for all the nonisotopic model variables have been obtained from the European Centre for Medium-Range Weather Forecasts (ECMWF) operational analysis data. For the considered period in July 2011 these data are available every 6 h with a spectral resolution of T1279 (≈20 km) and 91 vertical levels. For the isotope variables, data from the global isotope-enabled general circulation model IsoGSM (T62, 17 vertical levels) are used [*Yoshimura et al.*, 2008]. These data were produced by nudging the IsoGSM model to global reanalysis data [*Yoshimura et al.*, 2008; *Yoshimura and Kanamitsu*, 2008]. The chosen domain for the simulations in this study covers western continental Europe (see Figure 1).

In the following, we discuss $COSMO_{iso}$ simulations of the cold front passage on 24 July for which the model best represents the temporal evolution of the local rainfall at the point of measurement (Figure S5). The simulation period is from 12UTC 23 July to 12UTC 25 July. Obviously a correct simulation of the isotopic composition of near-surface vapor and precipitation depends strongly on the correct simulation of the mesoscale weather pattern. Note that the simulated meteorological evolution is the same in all sensitivity experiments, since the isotope parameterizations do not affect any other model components. Comparing the results from the experiments thus provides a quantitative estimate of the dependency of isotope signals in the model on important isotope parameterizations.

4.2. Comparison of Simulated and Measured Water Vapor Isotope Signals

Qualitatively, the role of the mesoscale weather system for the local-scale isotopic variability is evident from a comparison of $COSMO_{iso}$ results, featuring a more detailed representation of the regional dynamics, to the global model (IsoGSM), which represents only the large-scale climatological context. The δ_v values from IsoGSM are higher (20–50‰ for δ^2_vH and 3–7‰ for δ^{18}_vO) and show less variability than the measured signal (compare black and orange lines in Figures 3a and 3b). From IsoGSM, d_v stays nearly constant between

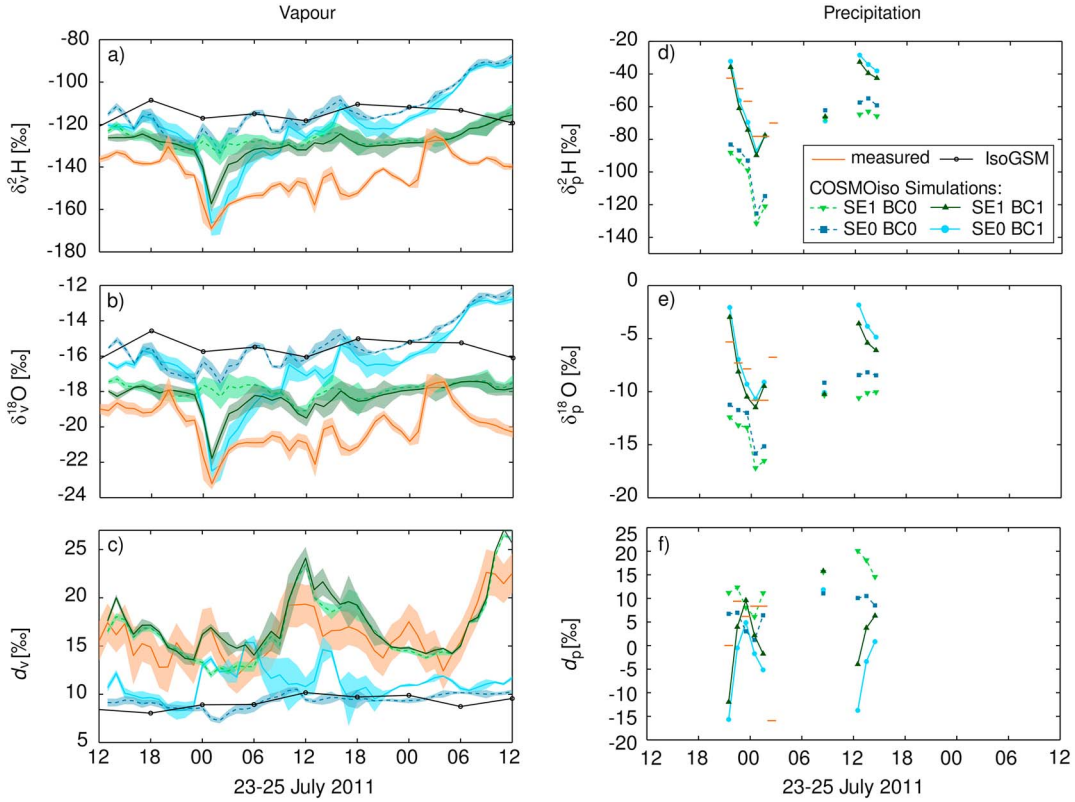

Figure 3. Comparison between measured (orange) and modeled (blue and green) (a–c) vapor and (d–f) precipitation isotope signals for the cold front passage at 00UTC 24 July 2011. In Figures 3a–3c, the measured hourly water vapor isotope signals are shown in orange with the shaded area indicating the measurement uncertainty range. The lowest model level water vapor isotope signals are taken from the $COSMO_{iso}$ simulations and interpolated bilinearly to the point of isotope measurement. The shaded area for the water vapor isotope simulations represents the standard deviation of the simulated isotope signals in a square of 56 km^2 around the isotope measurement station. In blue the simulations without fractionation during SE (SE0) are shown, and in green the simulations with SE fractionation following *Craig and Gordon* [1965] (SE1). Dashed lines show simulations without BC interaction (BC0), and solid lines simulations with BC interaction (BC1). The lowest model level water vapor isotope signals from the GCM used as boundary conditions (IsoGSM) [*Yoshimura et al.*, 2008] are shown in black. Date ticks show hours in UTC.

12UTC 23 July and 12UTC 25 July at a value of 10‰, which corresponds to the global average signature of meteoric water [*Craig*, 1961] (Figure 3c). The SE0BC0 $COSMO_{iso}$ simulation (dark blue line in Figures 3a–3c) shows slightly more variability than the global model, but is not in better agreement with the measurements, indicating that a refined representation of the weather system dynamics alone does not lead to a better representation of the water vapor isotope signal. Only by adding the microphysical processes related to BC interaction and the fractionation effects during SE (SE1BC1, dark green line in Figures 3a–3c) is the $COSMO_{iso}$ model able to more adequately represent the measured isotopic composition in the vapor. The correct amplitude of the V-shaped decrease in δ_v during the cold front passage around 00UTC 24 July can only be obtained if BC effects are included. The local interaction between rain droplets and vapor thus appear as an important controlling factor for the V shape in the δ_v signal pointing to an imprint of the falling rain on the ambient vapor. The lower measured δ_v values after the cold front passage associated with the colder northern European air mass are not adequately reproduced by the simulations, which may be due to a misrepresentation of the isotope fractionation at the moisture origin or the influence of the (biased) IsoGSM boundary data. The local maximum in d_v around 01UTC 24 July (discussed also in section 3.1) is only obtained in the BC1 simulations. This indicates that this feature may also result from BC interaction with rainfall.

Continental moisture sources played a prominent role with > 85% continental evaporation contributing to the water vapor arriving in Zurich during the passage of the cold front (computed using the moisture source diagnostics from *Sodemann et al.* [2008] and applied to water vapor as described in *Aemisegger et al.* [2014]).

This explains the strong impact that SE fractionation has on the near-surface water vapor isotope signal if it is activated in the model. The generally lower δ_v values seen in the measurements as well as the variability in d_v are much better reproduced in the SE1 simulations (Figures 3a–3c). Note that the better performance of $COSMO_{iso}$ in simulating d_v compared to the δ_v signals could result from the fact that even though the soil moisture δ_v values may be biased (too high), their ratio and thus also d_v is correct (here ≈ 10‰). Other possible explanations for the better agreement between simulation and observations for d_v than for δ_v is an underestimation of vertical mixing or of the rainout along the air parcel trajectory in $COSMO_{iso}$.

On 24 and 25 July a daily cycle in d_v with a minimum in the early morning hours and a maximum just before noon can be seen in the measurements and the SE1 simulations (Figure 3c), which is probably due to a high contribution of SE to the total evapotranspiration flux following precipitation in large parts of the continental moisture source region.

4.3. Comparison of Simulated and Measured Precipitation Isotope Signals

In all simulations, the temporal evolution of δ_p shows the V-shaped decrease as observed in the measurements (see Figures 3d and 3e). The fact that for both δ_p and δ_v the V-shaped decrease in the simulations and the observations agree well shows that the temporal evolution of the air mass rain out is correctly represented in the model. The V shape and absolute values of δ_p agree best with the measurements when including BC effects (solid lines in Figures 3d and 3e). Without BC effects, the BC enrichment of precipitation [*Dansgaard*, 1954; *Strong et al.*, 2007] does not take place, and the δ_p values underestimate the observations by 20–40‰ in δ_p^2H and by 5–10‰ in $\delta_p^{18}O$. Furthermore, the negative d_p cannot be simulated without BC interaction, confirming that on short time scales, d_p can be substantially influenced by local BC rainfall evaporation effects as previously shown [e.g., *Stewart*, 1975; *Barras and Simmonds*, 2009]. To illustrate the impact of BC evaporation on total precipitation an additional simulation was performed (RBC0) with the same setup as in SE1BC0 but with BC evaporation switched off for the isotopes and rainfall. The temporal evolution of precipitation and vapor isotopes remains nearly the same in the RBC0 as in the SE1BC0 experiment. However, the total amount of rainfall in the RBC0 simulation is increased by 74%. Even though the dynamical impact of BC evaporation on the temporal evolution of the event needs to be investigated in more detail, it appears that precipitation is considerably affected by BC processes both in terms of isotopic composition and precipitation amount reaching the surface.

The impact of SE fractionation on precipitation isotopes is negligible (compare blue and green lines in Figures 3d–3f). This may be partly due to the short simulation period. Indeed, the moisture at higher altitudes may not yet be affected by the different SE fractionation parameterizations. Nevertheless, our results indicate that BC interaction is an important process for isotopic variations in precipitation on short time scales. BC interaction probably largely sets the absolute δ_p values, whereas source effects and the transport dynamics define the temporal evolution.

4.4. Comparison of Simulated and Measured Disequilibrium

As expected, the disequilibrium between vapor and precipitation ($\delta_v - \delta_{veqp}$, Figure S6) is in best agreement with the measurements in the BC1 simulations. However, the relative enrichment of precipitation compared to near-surface vapor in the BC1 simulations is insufficient. This can be due to errors in the nonequilibrium fractionation factors or to deficiencies in the representation of the vertical structure of the front leading to errors in the vertical δ_v or relative humidity profiles (the latter causing insufficient BC enrichment).

4.5. Nonlinear Feedbacks

The difference between the strength of the BC interaction for SE1 and SE0 simulations illustrates the nonlinear feedbacks involved in these simulations. In the SE0BC1 simulation, the vapor is more depleted during the cold front passage than in the SE1BC1 simulation (compare light blue and dark green lines in Figures 3a and 3b). In the SE0BC1 simulation, the SE flux is equal to the soil moisture isotope composition. The signature of the fractionating SE flux in the case of the SE1BC1 simulation depends on both the soil moisture and the ambient vapor isotope composition. Low near-surface δ_v values imply a stronger isotope gradient toward the soil moisture isotope signature, which can lead to relatively enriched SE. This interaction is absent in the SE0BC1 simulation, which explains the lower δ_v values than in the SE1BC1 simulation during the frontal passage. For the case study presented here, the best model setup to reproduce the observations is to include both fractionation effects during BC interaction (BC1) and SE (SE1).

5. Conclusions

Simultaneous measurements of $\delta^{18}O$ and $\delta^{2}H$ in water vapor and liquid precipitation collected from frontal passages with high temporal resolution contain information on microphysical exchange processes between precipitation and water vapor below the clouds and the vertical structure of these midlatitude precipitation systems. In the case study of a cold front passage presented here, our simulations clearly showed that both BC interaction and isotopic fractionation effects resulting from SE must be included to obtain the best representation of measured isotope signals. A better process understanding and representation of the isotopic variability in regional and global isotope-enabled numerical models will provide insightful additional information on relevant processes in the water cycle. Other nonisotope model parameterizations like the strength of BC evaporation, which has been shown here to considerably impact the simulated rainfall amount or the representation of continental evaporation can also profit from high-frequency isotope measurements, since isotopes provide information that is not available in other traditional meteorological variables.

Acknowledgments
We thank Peter Plüss for technical help with the rainfall sampler, Kei Yoshimura for the IsoGSM data, and MeteoSwiss for providing access to their meteorological measurement data and ECMWF analyses. All data including measurements and model output are available from the authors upon request (franziska.aemisegger@usys.ethz.ch). This study was partly supported by the Swiss National Science Foundation (SNSF), grant P2EZP2_155603. We are grateful for the comments of two anonymous reviewers, which helped to improve our manuscript.

The Editor thanks two anonymous reviewers for their assistance in evaluating this paper.

References

Aemisegger, F., S. Pfahl, H. Sodemann, I. Lehner, S. I. Seneviratne, and H. Wernli (2014), Deuterium excess as a proxy for continental moisture recycling and plant transpiration, *Atmos. Chem. Phys.*, *14*, 4029–4054, doi:10.5194/acp-14-4029-2014.

Aemisegger, F., P. Sturm, P. Graf, H. Sodemann, S. Pfahl, A. Knohl, and H. Wernli (2012), Measuring variations of $\delta^{18}O$ and $\delta^{2}H$ in atmospheric water vapor using two commercial laser-based spectrometers: An instrument characterisation study, *Atmos. Meas. Tech.*, *5*, 1491–1511, doi:10.5194/amt-5-1491-2012.

Barras, V., and I. Simmonds (2009), Observation and modeling of stable water isotopes as diagnostics of rainfall dynamics over southeastern Australia, *J. Geophys. Res.*, *114*, D23308, doi:10.1029/2009JD012132.

Bowen, G. J., and J. Revenaugh (2003), Interpolating the isotopic composition of modern meteoric precipitation, *Water Resour. Res.*, *39*(10), 1299, doi:10.1029/2003WR002086.

Celle-Jeanton, H., R. Gonfiantini, Y. Travi, and B. Sol (2004), Oxygen-18 variations of rainwater during precipitation: Application of the Rayleigh model to selected rainfalls in Southern France, *J. Hydrol.*, *289*, 165–177, doi:10.1016/j.jhydrol.2003.11.017.

Coplen, T. B., P. J. Neiman, A. B. White, J. M. Landwehr, F. M. Ralph, and M. D. Dettinger (2008), Extreme changes in stable hydrogen isotopes and precipitation characteristics in a landfalling Pacific storm, *Geophys. Res. Lett.*, *35*, L21808, doi:10.1029/2008GL035481.

Coplen, T. B. (2011), Guidelines and recommended terms for expression of stable-isotope-ratio and gas-ratio measurement results, *Rapid Commun. Mass Spectrom.*, *25*, 2538–2560, doi:10.1002/rcm.5129.

Craig, H. (1961), Isotopic variations in meteoric waters, *Science*, *133*, 1702–1703, doi:10.1126/science.133.3465.1702.

Craig, H., and L. I. Gordon (1965), Deuterium and oxygen 18 variations in the ocean and marine atmosphere, in *Stable Isotopes in Oceanographic Studies and Paleotemperature*, edited by E. Togiorgi, pp. 9–130, Spoleto, Italy, Conisglio nazionale delle ricerche, Laboratorio di geologia nucleare, Pisa.

Dansgaard, W. (1954), The O^{18}-abundance in fresh water, *Geochim. Cosmochim. Acta*, *6*, 241–260, doi:10.1016/0016-7037(54)90003-4.

Dansgaard, W. (1964), Stable isotopes in precipitation, *Tellus*, *16*, 436–468, doi:10.1111/j.2153-3490.1964.tb00181.x.

Dawson, D. T., M. Xue, J. A. Milbrandt, and M. K. Yau (2010), Comparison of evaporation and cold pool development between single-moment and multimoment bulk microphysics schemes in idealized simulations of tornadic thunderstorms, *Mon. Weather Rev.*, *138*, 1152–1171, doi:10.1175/2009MWR2956.1.

Eugster, W., S. Perego, H. Wanner, A. Leuenberger, M. Liechti, M. Reinhardt, P. Geissbühler, M. Gempeler, and J. Schenk (1998), Spatial variation in annual nitrogen deposition in a rural region in Switzerland, *Environ. Pollut.*, *102*, 327–335, doi:10.1016/S0269-7491(98)80051-1.

Gedzelman, S. D., and J. R. Lawrence (1990), The isotopic composition of precipitation from 2 extratropical cyclones, *Mon. Weather Rev.*, *118*, 495–509, doi:10.1175/1520-0493(1990)118<0495:TICOPF>2.0.CO;2.

Gibson, J. J., S. J. Birks, and T. W. D. Edwards (2008), Global prediction of δ_A and $\delta^{2}H$-$\delta^{18}O$ evaporation slopes for lakes and soil water accounting for seasonality, *Global Biogeochem. Cycles*, *22*, GB2031, doi:10.1029/2007GB002997.

Grams, C. M., H. Binder, S. Pfahl, N. Piaget, and H. Wernli (2014), Atmospheric processes triggering the central European floods in June 2013, *Nat. Hazards Earth Syst. Sci.*, *14*, 1691–1702, doi:10.5194/nhess-14-1691-2014.

Grasselt, R., D. Schüttemeyer, K. Warrach-Sagi, F. Ament, and C. Simmer (2008), Validation of TERRA-ML with discharge measurements, *Meteorol. Z.*, *17*, 763–773, doi:10.1127/0941-2948/2008/0334.

Hoffmann, G., M. Werner, and M. Heimann (1998), Water isotope module of the ECHAM atmospheric general circulation model: A study on timescales from days to several years, *J. Geophys. Res.*, *103*(D14), 16,871–16,896, doi:10.1029/98JD00423.

Jasechko, S., Z. D. Sharp, J. J. Gibson, S. J. Birks, Y. Yi, and P. J. Fawcett (2013), Terrestrial water fluxes dominated by transpiration, *Nature*, *496*, 347–350, doi:10.1038/nature11983.

Lee, J. E., and I. Fung (2007), "Amount effect" of water isotopes and quantitative analysis of post-condensation processes, *Hydrol. Processes*, *22*, 1–8, doi:10.1002/hyp.6637.

Lee, X., S. Sargent, R. Smith, and B. Tanner (2005), In situ measurement of the water vapor 18O/16O isotope ratio for atmospheric and ecological applications, *J. Atmos. Oceanic Technol.*, *22*, 555–565, doi:10.1175/JTECH1719.1.

Majoube, M. (1971), Fractionnement en oxygne-18 et en deutrium entre l'eau et sa vapeur, *J. Chem. Phys.*, *68*, 1423–1436.

Miyake, Y., O. Matsubaya, and C. Nishihara (1968), An isotopic study on meteoric precipitation, *Pap. Meteorol. Geophys.*, *19*, 243–266.

Muller, C. L., A. Baker, I. J. Fairchild, C. Kidd, and I. Boomer (2015), Intra-event trends in stable isotopes: Exploring midlatitude precipitation using a vertically pointing micro rain radar, *J. Hydrometeorol.*, *16*, 194–213, doi:10.1175/JHM-D-14-0038.1.

Pfahl, S., H. Wernli, and K. Yoshimura (2012), The isotopic composition of precipitation from a winter storm: A case study with the limited-area model COSMOiso, *Atmos. Chem. Phys.*, *12*, 1629–1648, doi:10.5194/acp-12-1629-2012.

Prechsl, U. E., A. K. Gilgen, A. Kahmen, and N. Buchmann (2014), Reliability and quality of water isotope data collected with a low-budget rain collector, *Rapid Commun. Mass Spectrom.*, *28*, 879–885, doi:10.1002/rcm.6852.

Rindsberger, M., S. Jaffe, S. Rahamim, and J. R. Gat (1990), Patterns of the isotopic composition of precipitation in time and space: Data from the Israeli storm water collection program, *Tellus B*, *42*, 263–271, doi:10.1034/j.1600-0889.1990.t01-2-00005.x.

Risi, C., S. Bony, F. Vimeux, M. Chong, and L. Descroix (2008), Evolution of the stable water isotopic composition of the rain sampled along Sahelian squall lines, *Q. J. R. Meteorol. Soc.*, *136*, 227–242, doi:10.1002/qj.485.

Rossa, A., P. Nurmi, and E. Ebert (2008), Overview of methods for the verification of quantitative precipitation forecasts, in *Precipitation: Advances in Measurement, Estimation and Prediction*, edited by S. Michaelides, pp. 419–452, Springer, Berlin.

Sodemann, H., C. Schwierz, and H. Wernli (2008), Interannual variability of Greenland winter precipitation sources: Lagrangian moisture diagnostic and North Atlantic Oscillation influence, *J. Geophys. Res.*, *113*, D03107, doi:10.1029/2007JD008503.

Schrodin, R., and E. Heise, (2001), The multi-layer version of the DWD soil model TERRA_LM, Tech. Rep., Deutscher Wetterdienst, Offenbach am Main, Germany. [Available at http://www.cosmo-model.org/content/model/documentation/techReports/docs/techReport02.pdf.]

Spiegel, J. K., et al. (2012), Temporal evolution of stable water isotopologues in cloud droplets in a hill cap cloud in central Europe (HCCT-2010), *Atmos. Chem. Phys.*, *12*, 11,679–11,694, doi:10.5194/acp-12-11679-2012.

Steppeler, J., G. Doms, U. Schättler, H. W. Bitzer, A. Gassmann, U. Damrath, and G. Gregoric (2003), Meso-gamma scale forecasts using the nonhydrostatic model LM, *Meteorol. Atmos. Phys.*, *82*, 75–96, doi:10.1007/s00703-001-0592-9.

Stewart, M. K. (1975), Stable isotope fractionation due to evaporation and isotopic exchange of falling waterdrops: Applications to atmospheric processes and evaporation of lakes, *J. Geophys. Res.*, *80*(9), 1133–1146, doi:10.1029/JC080i009p01133.

Strong, M., Z. D. Sharp, and D. S. Gutzler (2007), Diagnosing moisture transport using D/H ratios of water vapor, *Geophys. Res. Lett.*, *34*, L03404, doi:10.1029/2006GL028307.

Winschall, A., S. Pfahl, H. Sodemann, and H. Wernli (2012), Impact of North Atlantic evaporation hot spots on southern Alpine heavy precipitation events, *Q. J. R. Meteorol. Soc.*, *138*, 1245–1258, doi:10.1002/qj.987.

Yoshimura, K., and M. Kanamitsu (2008), Dynamical global downscaling of global reanalysis, *Mon. Weather Rev.*, *136*, 2983–2998, doi:10.1175/2008MWR2281.1.

Yoshimura, K., M. Kanamitsu, D. Noone, and T. Oki (2008), Historical isotope simulation using reanalysis atmospheric data, *J. Geophys. Res.*, *113*, D19108, doi:10.1029/2008JD010074.

Yoshimura, K., M. Kanamitsu, and M. Dettinger (2010), Regional downscaling for stable water isotopes: A case study of an atmospheric river event, *J. Geophys. Res.*, *115*, D18114, doi:10.1029/2010JD014032.